nature photonics

LETTERS

https://doi.org/10.1038/s41566-022-01059-y

Check for updates

High-efficiency and broadband on-chip electro-optic frequency comb generators

Yaowen Hu[1,2,7]✉, Mengjie Yu[1,3,7], Brandon Buscaino[4], Neil Sinclair[1,5], Di Zhu[1], Rebecca Cheng[1], Amirhassan Shams-Ansari[1], Linbo Shao[1], Mian Zhang[6], Joseph M. Kahn[4] and Marko Lončar[1]✉

Developments in integrated photonics have led to stable, compact and broadband comb generators that support a wide range of applications including communications[1], ranging[2], spectroscopy[3], frequency metrology[4], optical computing[5,6] and quantum information[7,8]. Broadband optical frequency combs can be generated in electro-optical cavities, where light passes through a phase modulator multiple times while circulating in an optical resonator[9–12]. However, broadband electro-optic frequency combs are currently limited by low conversion efficiencies. Here we demonstrate an integrated electro-optic frequency comb with a conversion efficiency of 30% and an optical span of 132 nm, based on a coupled-resonator platform on thin-film lithium niobate[13]. We further show that, enabled by the high efficiency, the device acts as an on-chip femtosecond pulse source (336 fs pulse duration), which is important for applications in nonlinear optics, sensing and computing. As an example, in the ultrafast and high-power regime, we demonstrate a frequency comb with simultaneous electro-optic and third-order nonlinearity effects. Our device paves the way for practical optical frequency comb generators and provides a platform to investigate new regimes of optical physics that simultaneously involve multiple nonlinearities.

On-chip optical frequency comb (OFC) generators provide opportunities for robust, compact, portable and scalable comb sources, enabling a wide range of applications. So far, the majority of on-chip OFCs originate from continuous-wave (pump) light driving resonantly enhanced third-order optical nonlinearities ($\chi^{(3)}$) in the anomalous group velocity dispersion (GVD) regime, producing Kerr frequency combs[14]. Although these OFCs (typically referred to as bright-soliton Kerr combs) can feature attractive properties, such as octave-spanning bandwidths at terahertz-range comb line spacings, Kerr combs are limited by low pump-to-comb conversion efficiencies of a few percent, owing to the special mode-locking regime in which the pump is detuned far from the cavity resonance[15]. Improving the efficiency of Kerr combs using a coupled-resonator structure has also been investigated recently[16,17]. In contrast to bright-soliton Kerr combs, another approach for Kerr combs has recently emerged that relies on dark pulses[18–20]. Dark-pulse Kerr combs are generated in the normal GVD regime and can increase the conversion efficiency to ~10–50%. However, this comes at the expense of broader temporal widths, which renders them unsuitable for ultrafast (for example, femtosecond) pulse generation. Finally, a characteristic of all Kerr frequency combs is the existence of a pump threshold that is determined by both the Kerr nonlinearity and the quality factor (Q) of the resonator. This results in a nonlinear dependence between the comb and pump powers, which leads to saturation effects and limits the absolute comb power.

Electro-optic (EO) modulation provides an attractive alternative to OFC generation[9–12,21–23]. The electrical controllability of EO combs provides not only versatility but also excellent comb stability and phase coherence. EO combs based on conventional (travelling-wave) modulators feature a high pump-to-comb conversion efficiency, but their span is only a few nanometres due to the weak frequency mode interaction during a single pass through the modulator[21,22]. Wider optical combs can be generated using cavity-based EO combs in which light passes through a phase modulator multiple times while circulating inside an optical microresonator (Fig. 1a)[9–12,23,24] Recent progress on thin-film lithium niobate (TFLN) has enabled on-chip EO combs with a record-high optical span of ~80 nm (ref. [12]). However, the comb conversion efficiency of this single-resonator EO comb generation is limited to only ~0.3%. Such a low conversion efficiency originates from a strongly under-coupled 'hot' cavity resonance (<1% extinction ratio) when the generator is driven using a strong microwave tone. As a result, most of the light is not coupled into the resonator and is transmitted through the bus waveguide without entering the cavity (Fig. 1c).

Here we address the low conversion efficiency of the cavity-based EO comb and experimentally demonstrate an on-chip EO comb with a line spacing of 30.925 GHz, a pump-to-comb conversion efficiency of 30% and a wide comb span of 132 nm. This is enabled by two mutually coupled resonators (Fig. 1d) realized in the TFLN platform[13,25]. A small resonator (cavity 1) is used to over-couple only the pump mode of a racetrack cavity (cavity 2 for comb generation) while rejecting the other non-pump modes (Fig. 1e). This results in a critically coupled device when the microwave modulation is on (Fig. 1f) and increases the conversion efficiency as theoretically predicted[26,27]. Here in this work, we use the tight-binding model, previously developed for frequency crystals[28], as well as the generalized critical coupling (GCC) condition, developed for EO frequency shifters and beam splitters[13], to model our coupled-resonator EO comb generator. Importantly, our theoretical approach enables the derivation of an analytical solution for the system and can be extended to multiple coupled-resonator devices that may provide additional novel functionalities. Our experimental demonstration, along with the previous investigation of coupled-resonator

[1]John A. Paulson School of Engineering and Applied Sciences, Harvard University, Cambridge, MA, USA. [2]Department of Physics, Harvard University, Cambridge, MA, USA. [3]Ming Hsieh Department of Electrical and Computer Engineering, University of Southern California, Los Angeles, CA, USA. [4]Edward L. Ginzton Laboratory, Department of Electrical Engineering, Stanford University, Stanford, CA, USA. [5]Division of Physics, Mathematics and Astronomy, and Alliance for Quantum Technologies (AQT), California Institute of Technology, Pasadena, CA, USA. [6]HyperLight Corporation, Cambridge, MA, USA. [7]These authors contributed equally: Yaowen Hu, Mengjie Yu. ✉e-mail: yaowenhu@fas.harvard.edu; loncar@seas.harvard.edu

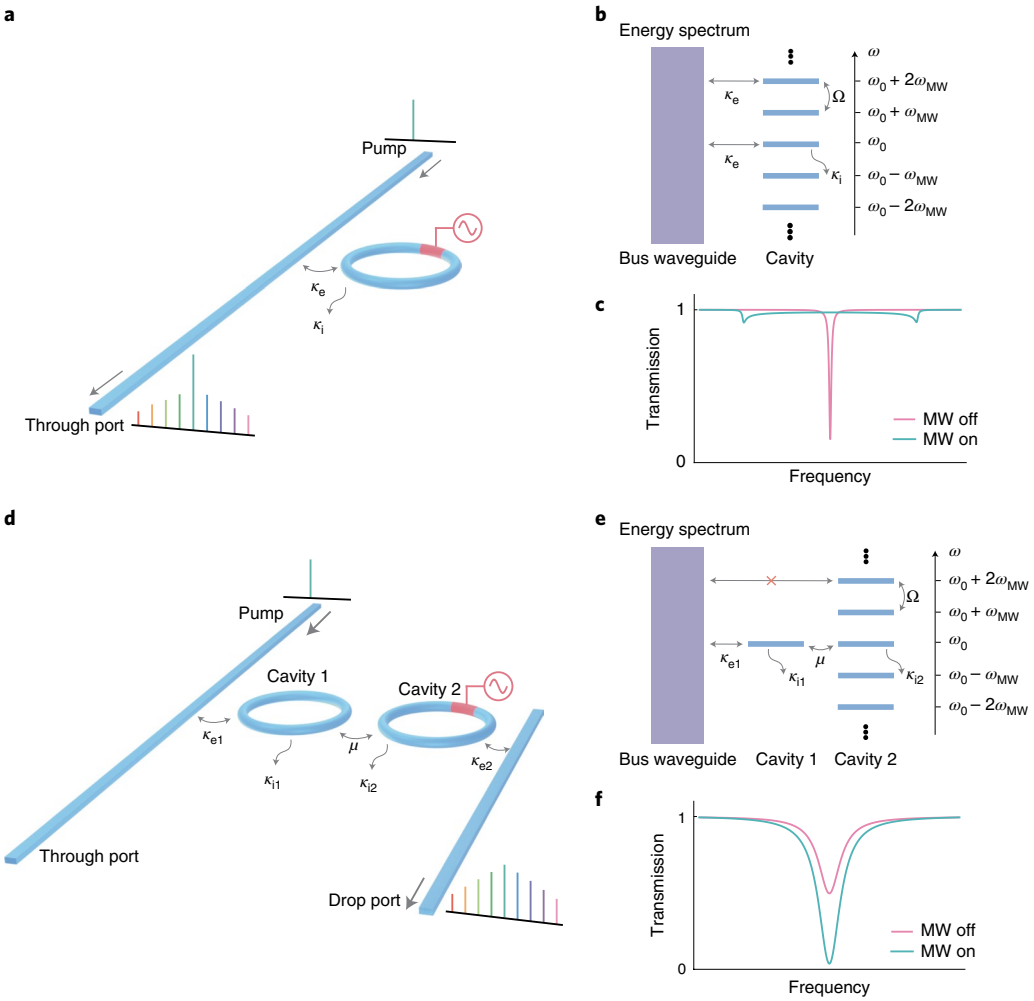

Fig. 1 | Concept of the coupled-resonator EO comb and GCC condition. a–c, Schematics of the device structure (**a**), energy-level description (**b**) and transmission spectrum (**c**) of the single-resonator EO frequency comb generator. EO modulation creates efficient coupling Ω between adjacent frequency modes of the cavity (**b**). All the frequency modes are coupled to the input bus waveguide. The rate κ_e is the waveguide–cavity coupling rate. When the microwave signal is off, the pump resonance is nearly critically coupled but becomes strongly under-coupled when the microwave signal is turned on. MW, microwave; ω_0, resonance frequency of the mode pumped by the laser; ω_{MW}, frequency of the microwave signal. **d–f**, Schematics of the device structure (**d**), energy-level description (**e**) and through-port transmission spectrum (**f**) of the coupled-resonator EO frequency comb generator. The inclusion of cavity 1 effectively causes an over-coupling between the pump mode of cavity 2 and the bus waveguide, while rejecting other frequency modes of cavity 2 (**e**). Such coupled-ring structures can achieve a GCC condition, resulting in a high extinction ratio of the pump resonance when the microwave signal is turned on (**f**). The rate κ_{e1} (κ_{e2}) is the coupling rate between the waveguide and cavity 1 (2). The coupling rate between cavities 1 and 2 is μ. The terms κ_{i1} and κ_{i2} are the intrinsic loss rates of cavity 1 and cavity 2, respectively.

Kerr comb generation[16], indicates that the coupled-resonator platform could be a general approach for power-efficient EO and Kerr comb sources.

The origin of the low conversion efficiency for single-resonator EO combs is the strong effective loss rate κ_{MW} for the pump mode, induced by the microwave modulation, which extracts power from the pump mode into other comb lines. The loss rate κ_{MW} is given in equation (1) (see the section 'Theoretical analysis' in the Methods):

$$\kappa_{MW} = \kappa\left(\sqrt{1+\frac{4\Omega^2}{\kappa^2}}-1\right) \quad (1)$$

where Ω is the mode-coupling rate between resonator modes separated by the free spectral range (FSR) and is proportional to the microwave voltage, and κ ($=\kappa_e+\kappa_i$) is the cavity loss rate, with κ_i and κ_e being the intrinsic loss and coupling rate to the bus waveguide, respectively. Here κ_{MW} can be orders of magnitude higher than κ_e and κ_i (for example, $\kappa_{MW} \approx 10$ GHz and $\kappa_e \approx \kappa_i \approx 100$ MHz for TFLN). Broadband EO combs require a strong microwave driving power (large Ω), which leads to a large κ_{MW}. This, however, results in the cavity being strongly under-coupled ($\kappa_e \ll \kappa_i + \kappa_{MW}$), reducing the comb efficiency. This trade-off between the EO comb span and the efficiency limits all single-resonator EO comb sources.

A coupled-resonator EO comb generator can overcome this trade-off and ensures efficient energy flow into the comb cavity (Fig. 1d). In this case, a critical coupling between the bus waveguide and the device can be achieved under the existence of the strong κ_{MW}, if the following condition, referred to as the GCC condition, is met (Fig. 1e,f):

$$\kappa_{e1} = \kappa_{i1} + \frac{4\mu^2}{\kappa_{e2}+\kappa_{i2}+\kappa_{MW}}$$

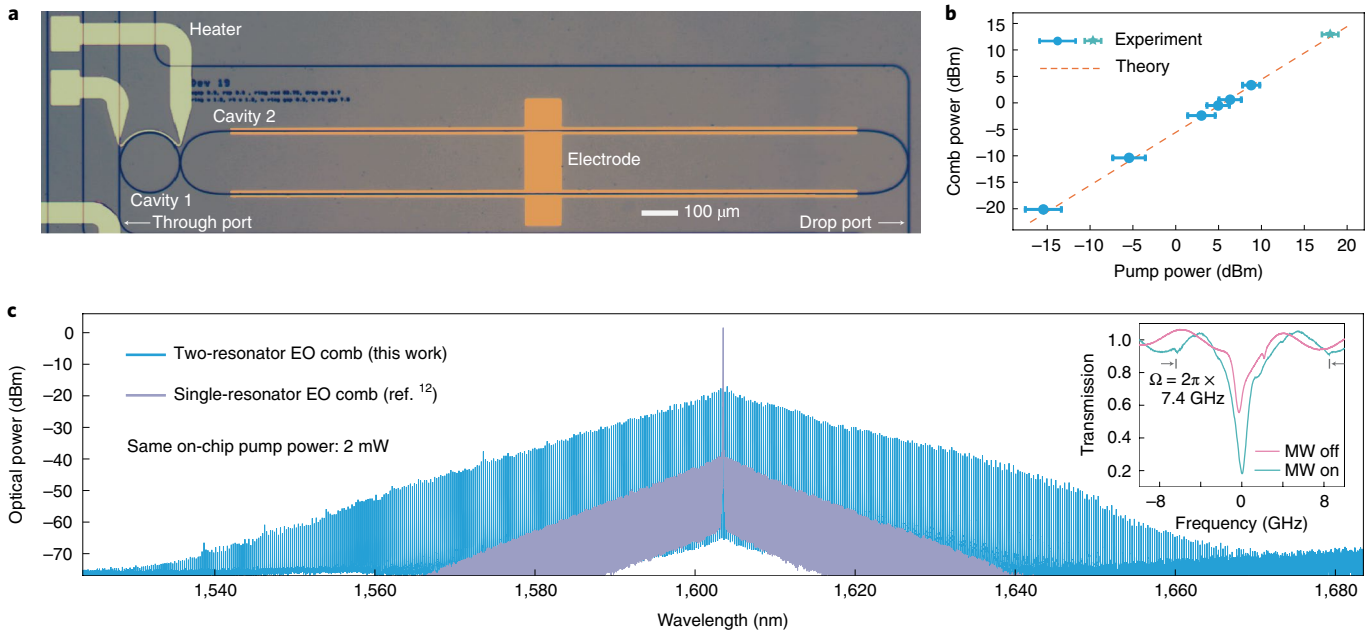

Fig. 2 | High-efficiency and broadband EO comb generator. a, Device optical image (false colour). Cavity 1 is controlled using a thermal heater (light yellow) and cavity 2 is modulated by a microwave signal applied to gold electrodes (orange). **b**, Measured comb power versus pump power, indicating a pump-to-comb conversion efficiency of 30%. The data points labelled as blue circles and the green diamond represent data from two different devices with the same parameters. Data points denoted as blue circles are for comb shapes similar to the comb in **c**, and the green diamond represents the nonlinear comb in the ultrafast high-power regime (see Fig. 4d). The error bars for each value of the pump power are due to Fabry–Perot fringes induced by the two facets of the chip. Each data point is obtained by averaging the maximum and minimum pump power values in the fringes. Therefore, the pump power $P_{in} = \frac{P_{in,max}+P_{in,min}}{2}$ with an error range of $P_{in,max} - P_{in,min}$. The theoretical curve is obtained based on the conversion efficiency formula $\eta = \frac{P_2}{P_{in}} \times \xi$ (see 'Theoretical analysis' section). **c**, Optical spectra of the coupled-resonator EO comb generator (blue, this work) and the single-resonator structure (purple, ref. [12]). Both spectra show the on-chip power. This is accomplished by taking into account the different in- and out-coupling facet losses to compare the spectra on the same footing, that is, for the same on-chip pump power of 2 mW. At a −70 dBm power level, the span of the coupled-resonator comb is 132 nm, whereas the span of the single-resonator EO comb[12] is 60 nm. The inset shows the transmission spectrum of the through port (see Fig. 1d) when the microwave signal is off (magenta) and on (cyan). The span between two shallow transmission dips (indicated by the grey vertical lines with arrows) is the conventional resonance broadening of the EO comb generator, which gives the coupling rate $2\Omega = 2 \times 2\pi \times 7.4$ GHz as well as the modulation index $\beta = 2\pi \frac{\Omega}{FSR} = 2\pi \frac{2\pi \times 7.4\ GHz}{2\pi \times 30.925\ GHz} = 0.48\pi$.

where κ_{e1} and κ_{e2} are the waveguide coupling rates between the bus waveguide and cavity 1 and between the output waveguide and cavity 2, respectively, κ_{i1} and κ_{i2} are the intrinsic loss rates for cavities 1 and 2, respectively, and μ is the coupling rate between cavities 1 and 2. The term $\frac{4\mu^2}{\kappa_{e2}+\kappa_{i2}+\kappa_{MW}} \equiv \kappa_{1eff}$ can be interpreted as an effective loss rate of cavity 1 that is induced by cavity 2, the microwave modulation and the output waveguide (drop port). With the expression for κ_{MW} (equation (1)), the coupled-resonator EO comb generator, which involves hundreds of frequency modes, can be simplified to a two-level system that can be solved for analytically. See the detailed discussion regarding the expression, and the maximum theoretical limitation, of efficiency in the 'Theoretical analysis' section.

To experimentally demonstrate the coupled-resonator comb generator, we fabricated TFLN-on-insulator devices (Fig. 2a). The small ring resonator and the long racetrack resonator are used as cavities 1 and 2, respectively. A microwave signal is sent to the electrode of cavity 2 to provide phase modulation. A thermal heater is used in cavity 1 for efficient resonance tuning.

We first demonstrate high-efficiency and broadband EO frequency comb generation. Continuous-wave light at 1,605 nm is fed into the device through the bus waveguide. A 30.925 GHz microwave signal, which matches the FSR of cavity 2, is used to drive the electrode. By applying microwave modulation, the transmission of the through port changes from over-coupled to nearly critically coupled (inset of Fig. 2c), indicating the efficient flow of pump power into the device. The frequency comb is collected at the drop port of the device (Fig. 1d) and measured using an optical spectrum analyser and photodetectors. The output comb power increases linearly with the pump power (Fig. 2b), indicating a pump-to-comb conversion efficiency of $\eta \equiv \frac{P_{comb}}{P_{pump}} = 30\%$, where P_{comb} and P_{pump} are the power values on the output and input waveguides, respectively. Using 2 mW of pump power (the same pump power as used in ref. [12]), the comb spans 132 nm at a −70 dBm power level and features an efficiency $\eta = 30\%$ (Fig. 2c). Our device can be pumped at any of the resonances of cavity 2 by tuning the heater to overlap the resonance of cavities 1 and 2 (see Extended Data Fig. 1). The current pump wavelength is ~1,600 nm. It is chosen to avoid the polarization mode crossing at ~1,400 nm, which can be suppressed via dispersion engineering (see Extended Data Fig. 2). Compared with state-of-the-art integrated EO combs[12], our method yields a two-orders-of-magnitude improvement in the conversion efficiency and a 2.2 times wider span is measured at the −70 dBm power level with the same pump power (Fig. 2c). It should be noted that in the single-resonator TFLN EO comb generator[12], the pump intensity is 40 dB higher than the first comb line due to the low efficiency from the strong under-coupling of the resonator (purple trace in Fig. 2c). For our coupled-resonator device, the output spectrum in the through port (residual pump) is discussed later in Fig. 3.

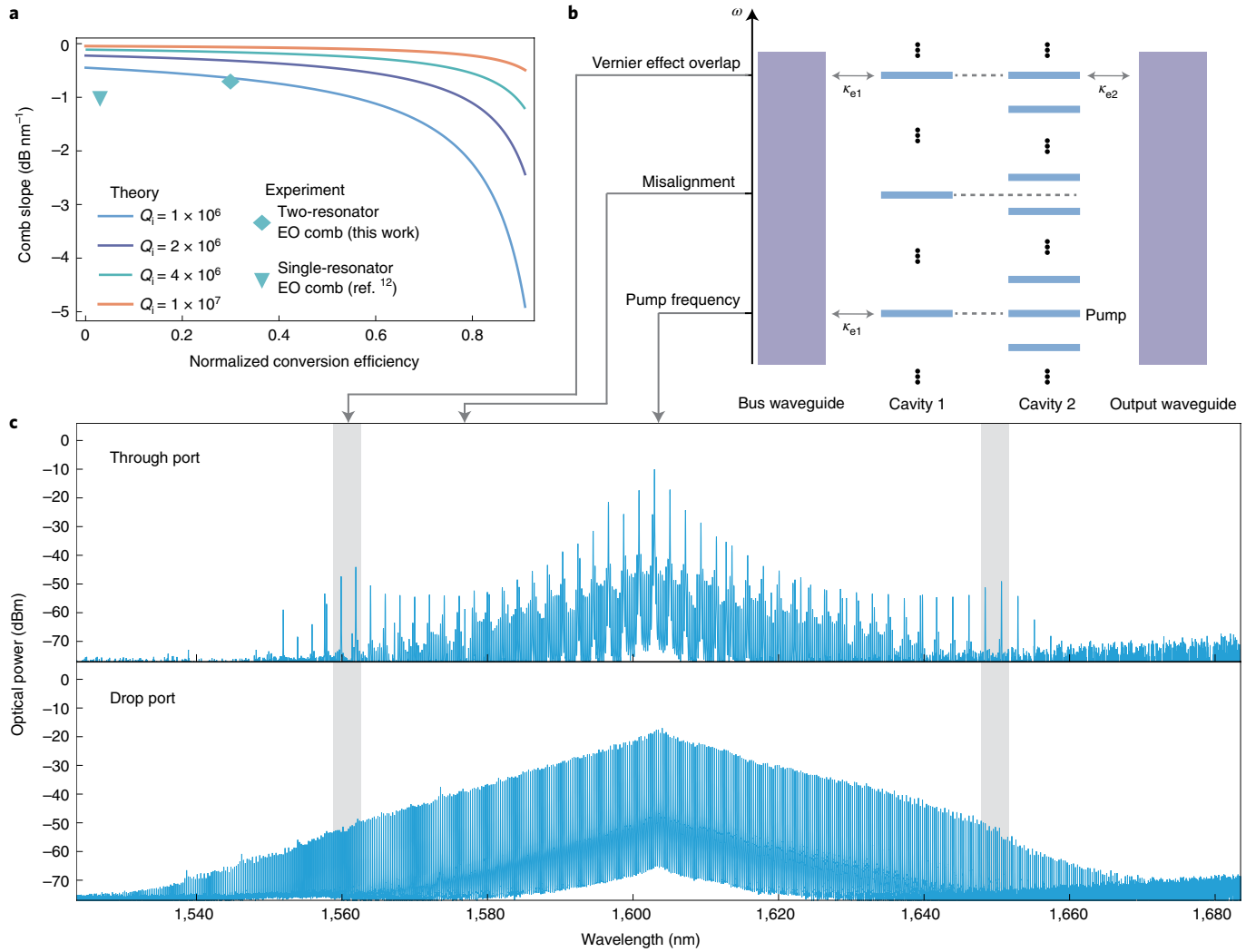

Fig. 3 | Theoretical analysis of conversion efficiency and the experimental optimization of mode-crossing effect. a, The comb slope versus the conversion efficiency η for different waveguide–cavity 2 coupling κ_{e2} and intrinsic quality factor Q_{i2} values. Each curve is generated by calculating η_{max} and the slope with κ_{e2} varied from $0 \times \kappa_{i2}$ to $10 \times \kappa_{i2}$. The intrinsic loss rate κ_{i2} is determined via the intrinsic quality factor Q_{i2}. The rate κ_{i2} (as well as Q_{i2}) is fixed for data points in each curve and varied for data points between different curves. Experimental data points in this figure represent the measured efficiency η, while theoretical data points use the theoretical upper limit of the efficiency η_{max}. **b**, Illustration of the Vernier effect for optimizing mode-crossing-induced loss using an energy-level diagram. Cavity 1 is designed to have its resonance aligned with the pump frequency of cavity 2 and is misaligned across a wide range of other frequencies. This overcomes the losses that would otherwise be induced by mode crossing. The through-port comb line will have a higher power close to the overlap area (grey shaded region in **c**) and vice versa. **c**, Output spectrum from the through port and drop port of the device shown in Fig. 2c. The shape of the through-port spectrum reflects how the Vernier effect of the cavity resonances of two rings affects the output comb in both the through port and the drop port. The final optimized device FSR values are 254.54 GHz (cavity 1) and 30.925 GHz (cavity 2).

To compare the performance between the existing frequency comb generators, we summarized the metrics of demonstrated EO and Kerr frequency combs in Table 1.

The conversion efficiency η can be understood by decomposing η into two components:

$$\eta = \theta \times \xi$$

where $\theta = \frac{P_2}{P_{in}}$ is the ratio between the optical power P_2 that flows into cavity 2 and the input power P_{in}, and $\xi = \frac{\kappa_{e2}}{\kappa_{e2}+\kappa_{i2}}$ with κ_{e2} and κ_{i2} being the waveguide–cavity 2 coupling rate and the intrinsic loss rate of cavity 2, respectively (see 'Theoretical analysis' section). The power ratio θ is determined by the GCC condition. When the GCC condition is met and when $\kappa_{e1} \gg \kappa_{i1}$, we have $\theta \approx 1$. The factor ξ describes how much power from cavity 2 is coupled into the output waveguide, which sets the theoretical upper limit for the conversion efficiency η_{max} for each device. It also generates a fundamental trade-off between the comb span and the conversion efficiency: for large ξ the comb generated inside cavity 2 can be efficiently coupled to the output waveguide, but at the same time the slope of the comb spectrum is increased due to the reduced lifetime of cavity 2, which leads to a lower loaded-quality factor of cavity 2. We theoretically obtained η_{max} and the slope of the comb for a range of κ_{e2} and intrinsic quality factor Q_{i2} for cavity 2 (which corresponds to κ_{i2}) to show this trade-off (Fig. 3a). Our comb (Fig. 2b) features a slope of -0.7 dB nm^{-1} and a measured efficiency of 30% ($\eta = 28\%$ in theory and simulation), which is close to $\eta_{max} = 38\%$ of our device. With an improved quality factor of 1×10^7, it is possible to obtain $\eta_{max} = 83\%$ with a slope of -0.27 dB nm^{-1} or $\eta_{max} = 50\%$ with a slope of -0.09 dB nm^{-1}. The difference between the achieved efficiency

Table 1 | Comparison of EO and Kerr frequency comb generators

Reference	Efficiency (%)	Pump power (mW)	Span (nm)	Repetition rate (GHz)	Number of comb lines[a]	Platform	Mechanism	Pump wavelength (nm)	Device size (mm²)
This work	30	2	132[b]	30.925	533	TFLN	EO; CR	1,600	0.5
	32	63	161		650		EO-Kerr; CR	1,550	
Zhang et al. (2019)[12]	~0.3[c]	2	60[b]	10.453	714	TFLN	EO; SR	1,600	1.2
Yi et al. (2015)[32]	~0.27	200	90	22	500	Silica	Kerr; BS; SR	1,550	N/A
	~0.7	50	60		333				
Marin-Palomo et al. (2017)[1]	0.1–0.6	1,000	>250[d]	>96	>325	SiN	Kerr; BS; SR	1,550	0.2
Liu et al. (2018)[33]	1.5	50.6	120	86	174	SiN	Kerr; BS; SR	1,550	0.2
Xue et al. (2019)[16]	0.0046	270	~6.4	0.003	~266,667	Fibre	Kerr; BS; CR	1,550	N/A[e]
Xue et al. (2017)[34]	31.8	656	~250	231	~135	SiN	Kerr; DP; SR	1,550	0.1
Kim et al. (2019)[19]	41	180	>120[f]	201.6	>75	SiN	Kerr; DP; CR	1,550	N/A
Helgason et al. (2021)[20]	32–49	13–18	~90	105	~107	SiN	Kerr; DP; CR	1,550	N/A
	36	2.5	~70	227	~39				0.5
Kourogi et al. (1993)[9]	N/A	N/A	32	5.8	690	Bulk	EO; SR	1,550	N/A
Xiao et al. (2008)[10]	N/A	N/A	~38[b]	10	~475	Bulk	EO; SR	1,560	N/A
Rueda et al. (2019)[11]	N/A	N/A	13[b]	8.9	186	WGM LN disk	EO; SR (with MW cavity)	1,550	N/A

CR, coupled resonator; SR, single resonator; BS, bright soliton; SiN, silicon nitride; DP, dark pulse; WGM, whispering gallery mode; LN, lithium niobate. The sequence of references is determined by the mechanism: EO comb, BS Kerr comb and DP Kerr comb. EO combs that are related but do not report efficiencies are listed at the end. [a]Number of comb lines calculated via the spanning/repetition rate. [b]Span defined at the −70 dBm power level. [c]Not reported in ref. [12], so extracted from the raw data in ref. [12]. [d]Full bandwidth is not shown. [e]The roundtrip lengths of the two fibre cavities are 1.8 m and 75.3 m. [f]For the comb with the quoted efficiency, its span is estimated to be slightly larger than 120 nm.

η and the theoretical efficiency η_{max} is due to the imperfect GCC condition, the non-zero value of κ_{i1} and the mode-crossing-induced loss due to cavity 1 (see below).

Cavity 1 has a large number of frequency modes that can lead to mode crossing with the modes of cavity 2, potentially causing comb power loss. To overcome this, we use an optimization algorithm to design the FSR values of cavities 1 and 2 so that they have overlapping resonances at the pump frequency only and misaligned resonances for most other frequencies (Vernier effect, Fig. 3a). To verify this, we collect the generated combs from both the through port and the drop port. The comb profile measured at the through port clearly shows the optimized Vernier effect (top third of Fig. 3b) and the spectrum at the drop port preserves the linear slope (bottom third of Fig. 3b) without cut-off[26], indicating that the mode-crossing loss is minimized. The profile of the comb collected at the through port is the result of the comb generation inside cavity 2 followed by 'cavity filtering' in cavity 1. This signal can also be useful for, for example, heterodyne measurements, as local oscillators or clock references.

Next, enabled by the high-efficiency and wide comb span, we demonstrate that the device can serve as an on-chip ultrafast pulse source, which is important for nonlinear applications such as broadband parametric frequency conversion and optical atomic clocks. To characterize the time-domain signal of the output frequency comb, the optical output is sent to an erbium-doped fibre amplifier (EDFA) and dispersion-compensating fibre (DCF) followed by a second-harmonic generation-based intensity autocorrelator (see Fig. 4a for the setup). The full-width at half-maximum (FWHM) of the autocorrelator trace is 1.072 ps, which corresponds to a pulse FWHM of 536 fs (Fig. 4b). We infer that the pulse FWHM in the output facet of the chip is around 336 fs after extracting the total dispersion of the fibre output path of 36 fs nm^{-1}. The two sidelobes near the Lorentzian-shaped pulse are caused by the non-uniform gain coefficient of our EDFA (see the section 'Pulse characterization' in the Methods).

Finally, we demonstrate the observation of EO and $\chi^{(3)}$ combined high-power frequency combs in a single device, enabled by the formation of ultrafast pulses with a high circulating peak power inside the resonator. To demonstrate this effect, a 63 mW pump power (in the bus waveguide) is used to feed the device (see the setup in Fig. 4a) and the output frequency comb features a 32% conversion efficiency, a 20 mW on-chip comb power and a broadened span of 161 nm (Fig. 4d). As a result, we infer that an estimated ~85 W peak pulse power (~1 W average power) is circulating inside the comb resonator (cavity 2) (see the section 'Frequency comb characterization' in the Methods), large enough to stimulate the additional Raman[29] and four-wave mixing effects[14] (Fig. 4e). Optimizing the dispersion of the current device from normal dispersion to anomalous dispersion could further enhance the four-wave mixing effect, which could be useful for ultrabroad comb generation. Combining $\chi^{(2)}$ and $\chi^{(3)}$ nonlinearities also provides an intriguing opportunity for investigating new regimes of nonlinear optical dynamics such

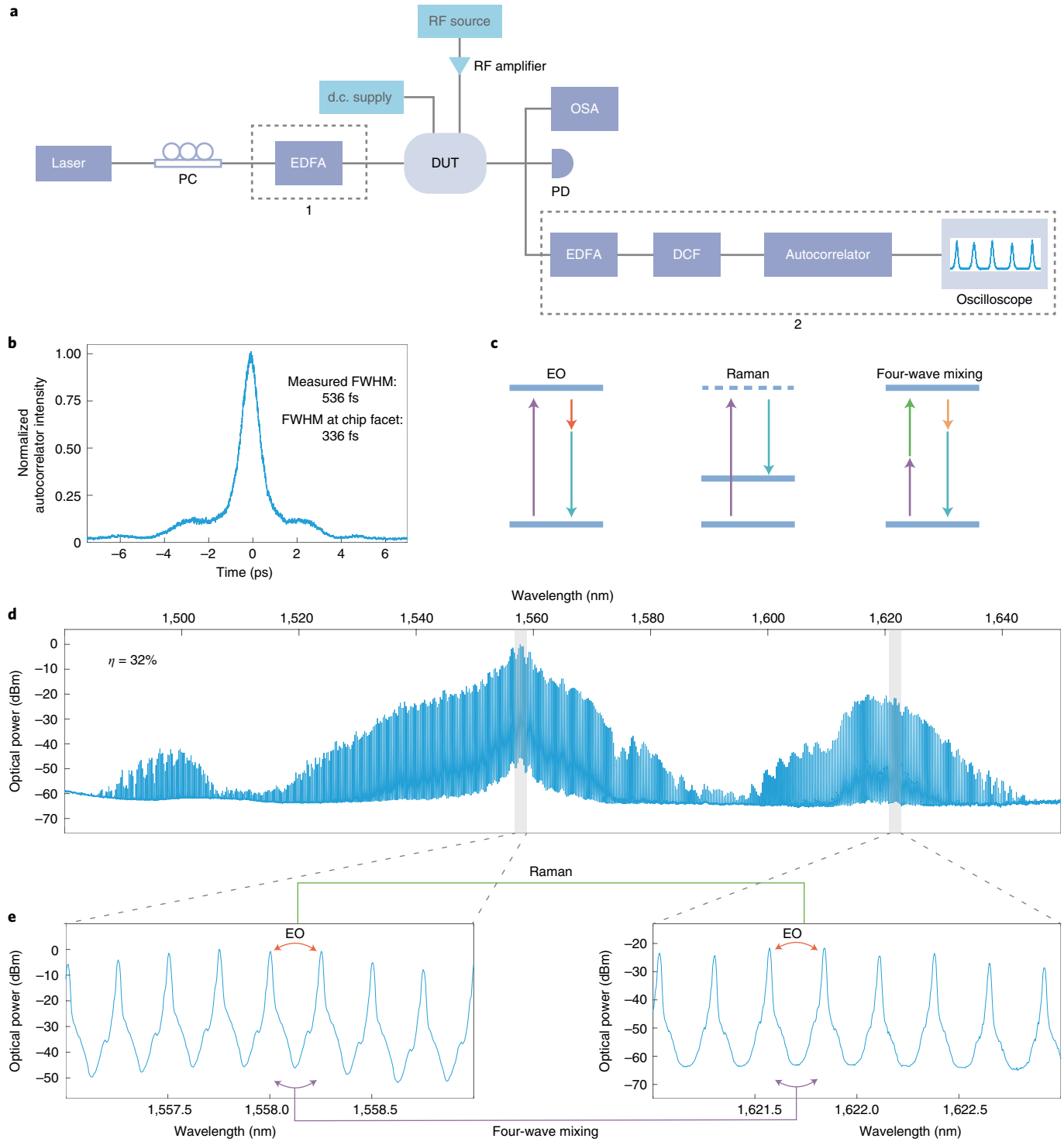

Fig. 4 | Femtosecond pulse source and multiple-combined nonlinearity in ultrafast high-power regime. a, Measurement setup. To characterize generated pulses in the time domain, the dashed box 2 is used. Dashed box 1 is used only when evaluating the high-power performance of the device. RF, radio frequency; d.c., direct current; OSA, optical spectrum analyser; PC, polarization controller; DUT, device under test; PD, photodetector. **b**, Time-domain trace of the output comb measured using an autocorrelator. The measured pulse FWHM is 536 fs, indicating a FWHM of 336 fs in the output facet of the chip after extracting the total dispersion of the fibre output path of 36 fs nm^{-1}. **c**, Illustration of the EO (left), Raman (middle) and four-wave mixing (right) effect. **d**, Device output spectrum that contains both the EO and $\chi^{(3)}$ effect when pumped using a high input power. The span is broadened to 161 nm due to Raman and four-wave mixing and the conversion efficiency is 32%. **e**, Illustration of the contained EO, Raman and four-wave mixing nonlinear processes.

as the proposed 'band soliton'[30] and might enable superior OFCs, owing to the ability to reach both the ultrafast and high-power regimes in the same resonator under EO modulation.

In summary, we demonstrate high-efficiency and broadband EO frequency combs using a coupled-resonator structure. We show that it can be used as an integrated femtosecond pulse source and can

stimulate combined second- and third-order nonlinear processes in the ultrafast high-power regime. In addition, we provide a theoretical model that simplifies the coupled-resonator system supporting hundreds of energy levels as a two-level system. Simultaneously achieving a high-efficiency and wide span can enable a broad range of applications. For example, an already demonstrated 100-fold improvement in comb efficiency can lead to a 20 dB increase in the signal-to-noise ratio of frequency-multiplexed applications such as optical communications[1]. These advances can also reduce the optical pump power needed for the realization of optical neural networks[5,6]. In addition, the microwave-power consumption could be reduced by integrating on-chip microwave resonators with our comb source. Furthermore, the ability to generate on-chip femtosecond pulses is important for nonlinear photonics, optical atomic clocks, optical sensing and time-bin-encoded optical computing. Finally, the high conversion efficiency of our device opens the door for a generation of broad EO combs for entangled photons, broadly enabling frequency-domain quantum information processing[28,31].

Online content

Any methods, additional references, Nature Research reporting summaries, source data, extended data, supplementary information, acknowledgements, peer review information; details of author contributions and competing interests; and statements of data and code availability are available at https://doi.org/10.1038/s41566-022-01059-y.

Received: 8 February 2022; Accepted: 13 July 2022;
Published online: 29 August 2022

References

1. Marin-Palomo, P. et al. Microresonator-based solitons for massively parallel coherent optical communications. *Nature* **546**, 274–279 (2017).
2. Suh, M. G. & Vahala, K. J. Soliton microcomb range measurement. *Science* **359**, 884–887 (2018).
3. Picqué, N. & Hänsch, T. W. Frequency comb spectroscopy. *Nat. Photonics* **13**, 146–157 (2019).
4. Papp, S. B. et al. Microresonator frequency comb optical clock. *Optica* **1**, 10–14 (2014).
5. Xu, X. et al. 11 TOPS photonic convolutional accelerator for optical neural networks. *Nature* **589**, 44–51 (2021).
6. Feldmann, J. et al. Parallel convolutional processing using an integrated photonic tensor core. *Nature* **589**, 52–58 (2021).
7. Kues, M. et al. Quantum optical microcombs. *Nat. Photonics* **13**, 170–179 (2019).
8. Lukens, J. M. & Lougovski, P. Frequency-encoded photonic qubits for scalable quantum information processing. *Optica* **4**, 8–16 (2016).
9. Kourogi, M., Ken'ichi, N. & Ohtsu, M. Wide-span optical frequency comb generator for accurate optical frequency difference measurement. *IEEE J. Quantum Electron.* **29**, 2693–2701 (1993).
10. Xiao, S., Hollberg, L., Newbury, N. R. & Diddams, S. A. Toward a low-jitter 10 GHz pulsed source with an optical frequency comb generator. *Opt. Express* **16**, 8498–8508 (2008).
11. Rueda, A., Sedlmeir, F., Kumari, M., Leuchs, G. & Schwefel, H. G. L. Resonant electro-optic frequency comb. *Nature* **568**, 378–381 (2019).
12. Zhang, M. et al. Broadband electro-optic frequency comb generation in a lithium niobate microring resonator. *Nature* **568**, 373–377 (2019).
13. Hu, Y. et al. On-chip electro-optic frequency shifters and beam splitters. *Nature* **599**, 587–593 (2021).
14. Kippenberg, T. J., Gaeta, A. L., Lipson, M. & Gorodetsky, M. L. Dissipative Kerr solitons in optical microresonators. *Science* **361**, eaan8083 (2018).
15. Bao, C. et al. Nonlinear conversion efficiency in Kerr frequency comb generation. *Opt. Lett.* **39**, 6126–6129 (2014).
16. Xue, X., Zheng, X. & Zhou, B. Super-efficient temporal solitons in mutually coupled optical cavities. *Nat. Photonics* **13**, 616–622 (2019).
17. Helgason, Ó. B. et al. Power-efficient soliton microcombs. Preprint at https://arxiv.org/abs/2202.09410 (2022).
18. Xue, X. et al. Mode-locked dark pulse Kerr combs in normal-dispersion microresonators. *Nat. Photonics* **9**, 594–600 (2015).
19. Kim, B. Y. et al. Turn-key, high-efficiency Kerr comb source. *Opt. Lett.* **44**, 4475–4478 (2019).
20. Helgason, Ó. B. et al. Dissipative solitons in photonic molecules. *Nat. Photonics* **15**, 305–310 (2021).
21. Sakamoto, T., Kawanishi, T. & Izutsu, M. Asymptotic formalism for ultraflat optical frequency comb generation using a Mach–Zehnder modulator. *Opt. Lett.* **32**, 1515–1517 (2007).
22. Ozharar, S., Quinlan, F., Ozdur, I., Gee, S. & Delfyett, P. J. Ultraflat optical comb generation by phase-only modulation of continuous-wave light. *IEEE Photonics Technol. Lett.* **20**, 36–38 (2008).
23. Ho, K.-P. & Kahn, J. M. Optical frequency comb generator using phase modulation in amplified circulating loop. *IEEE Photonics Technol. Lett.* **5**, 721–725 (1993).
24. Shams-Ansari, A. et al. An integrated lithium-niobate electro-optic platform for spectrally tailored dual-comb spectroscopy. *Commun. Phys.* **5**, 88 (2022).
25. Zhu, D. et al. Integrated photonics on thin-film lithium niobate. *Adv. Opt. Photonics* **13**, 242–352 (2021).
26. Buscaino, B., Zhang, M., Lončar, M. & Kahn, J. M. Design of efficient resonator-enhanced electro-optic frequency comb generators. *J. Lightwave Technol.* **38**, 1400–1413 (2020).
27. Kourogi, M., Enami, T. & Ohtsu, M. A coupled-cavity monolithic optical frequency comb generator. *IEEE Photonics Technol. Lett.* **8**, 1698–1700 (1996).
28. Hu, Y., Reimer, C., Shams-Ansari, A., Zhang, M. & Lončar, M. Realization of high-dimensional frequency crystals in electro-optic microcombs. *Optica* **7**, 1189–1194 (2020).
29. Yu, M. et al. Raman lasing and soliton mode-locking in lithium niobate microresonators. *Light Sci. Appl.* **9**, 9 (2020).
30. Tusnin, A. K., Tikan, A. M. & Kippenberg, T. J. Nonlinear states and dynamics in a synthetic frequency dimension. *Phys. Rev. A* **102**, 023518 (2020).
31. Imany, P., Lingaraju, N. B., Alshaykh, M. S., Leaird, D. E. & Weiner, A. M. Probing quantum walks through coherent control of high-dimensionally entangled photons. *Sci. Adv.* **6**, eaba8066 (2020).
32. Yi, X., Yang, Q.-F., Yang, K. Y., Suh, M.-G. & Vahala, K. Soliton frequency comb at microwave rates in a high-*Q* silica microresonator. *Optica* **2**, 1078–1085 (2015).
33. Liu, J. et al. Ultralow-power chip-based soliton microcombs for photonic integration. *Optica* **5**, 1347–1353 (2018).
34. Xue, X., Wang, P. H., Xuan, Y., Qi, M. & Weiner, A. M. Microresonator Kerr frequency combs with high conversion efficiency. *Laser Photon. Rev.* **11**, 1600276 (2017).

Methods

Device fabrication. Our devices are fabricated from a commercial X-cut lithium niobate on insulator wafer (NanoLN), with a 600 nm LN layer, 2 μm buried oxide (thermally grown), on a 500 μm silicon handle. Electron-beam lithography with a hydrogen silsesquioxane resist followed by argon-ion-based reactive ion etching (350 nm etch depth) are used to pattern the optical layer of the devices, including the rib waveguides and micro-ring resonators. The devices are cleaned and the microwave electrodes (15 nm of titanium, 300 nm of gold) are defined using photolithography followed by electron-beam evaporation and a bilayer lift-off process. One layer of silica (SiO_2) (800 nm) using plasma-enhanced chemical vapour deposition is used to clad the devices. The heater (15 nm of titanium and 200 nm platinum) for cavity 1 is defined by photolithography followed by electron-beam evaporation and lift-off. The heater is designed as a short metal strip (5 μm wide) that is placed 3 μm away from the resonator on top of the SiO_2 cladding. The resistance of the heater is ~140 Ω (including parasitic resistance from routing strips). Tuning of the ring resonance via the FSR is achieved using a current of ~50 mA.

Frequency comb characterization. The measurement setup is illustrated in Extended Data Fig. 3. Telecommunication-wavelength light from a fibre-coupled tunable laser (TSL-510, SANTEC) passes through a polarization controller and is coupled to the LN chip using a lensed fibre. The output is collected using a lensed fibre and then sent to an optical spectrum analyser with a spectral resolution of 0.02 nm for characterization of the frequency comb. The microwave signal is generated from a synthesizer followed by a microwave amplifier and delivered to the electrodes on a device using an electric probe. The microwave driving power is 2.2 W.

The circulating power in Fig. 4d is inferred from the comb power $P_{comb}=20$ mW in the bus waveguide, which for cavity 2 gives an intra-cavity power of: $P_{intra} = P_{comb} \times \frac{Finesse}{\pi}$. The Finesse is calculated using $Finesse = \frac{\kappa_2}{FSR_2} = \frac{222\ MHz}{30.925\ GHz} = 139.3$. Therefore $P_{intra}=0.9$ W and the peak power of the pulse can be inferred via $P_{peak} = \frac{t_{RT}}{\tau} P_{intra} = 85$ W in which $t_{RT}=32$ ps and $\tau=336$ fs are the roundtrip time of cavity 2 and the pulse duration, respectively.

The device parameters are extracted based on measurement on the transmission spectra (Extended Data Fig. 4 and Extended Data Table 1). The parameters of cavity 1 (κ_{e1} and κ_{i1}) and cavity 2 (κ_{e2} and κ_{i2}) are obtained from the linewidth and extinction ratio of the resonances. The coupling μ between the two cavities is extracted by tuning the two resonances of the cavities to a degenerate point and measuring the mode splitting, which gives $\mu = \sqrt{\left(\frac{Splitting}{2}\right)^2 + \left(\frac{\mu_{EP}}{2}\right)^2}$ where $\mu_{EP} = \frac{\kappa_1 - \kappa_2}{2}$ is the coupling strength required to reach the exceptional point of the system.

Pulse characterization. The output frequency comb is sent to an EDFA and a DCF followed by a second-harmonic generation-based intensity autocorrelator. The total dispersion of the optical path from the chip output facet to the autocorrelator (without the DCF) is characterized to be equivalent to the dispersion of a 12-m-long single-mode fibre (SMF-28, Thorlabs). The added DCF offsets the total dispersion to be equivalent to the dispersion of a 2 m SMF-28 fibre (36 ps nm^{-1} km^{-1}). The FWHM of the autocorrelator trace is 1.072 ps, which corresponds to a pulse FWHM duration of 536 fs (Fig. 4b). Therefore, the pulse FWHM duration at the output facet of the chip is inferred as 336 fs via extracting the total dispersion of the optical path (2 m SMF-28).

We note that the comb spectrum changes after the light passes the EDFA (Extended Data Fig. 5) due to the non-uniform gain spectrum of the EDFA, which might change the pulse duration and pulse shape. To confirm that our measurement reflects the true pulse duration, we analysed the spectrum before and after the EDFA. In this measurement, we used a device with similar parameters and performance to the device shown in Fig. 2. The slope of the spectrum is 1.0 dB nm^{-1} before the EDFA. After passing the EDFA, it is difficult to get an accurate spectral slope due to the non-uniform gain of the EDFA. However, the 3 dB bandwidth remains the same (3.75 nm). Since the pulse duration is mainly determined by the 3 dB bandwidth of the frequency comb, we infer that the pulse duration should be the same for the comb before and after the EDFA. To verify this, we first calculate the Lorentzian pulse duration for our pulse with the centre wavelength of 1,553.6 nm and the 3 dB bandwidth of 3.75 nm and obtain a pulse duration of 304 fs. We then perform a numerical simulation using the Heisenberg–Langevin equations to simulate the pulse duration for the EO comb with a slope of 1.0 dB nm^{-1} and find a simulated pulse duration of 316 fs. Both results are consistent with the measured pulse duration of 336 fs.

We also note that the non-uniform gain of the EDFA creates a bump on the left side of the comb. However, this bump is below the 9 dB bandwidth of the comb, so it should have little effect on the pulse duration. Nonetheless, this bump could distort the shape of the pulse from a perfect Lorentzian, and in the experiment we indeed observed a distortion of the pulse shape from the Lorentzian shape (sidelobes in Fig. 4b). We also measured the dual-pulse dynamics of the EO comb with varied optical detuning (Extended Data Fig. 6).

Theoretical analysis. *Effective loss rate induced by microwaves for the EO comb.* To obtain the effective loss rate that is induced by microwave modulation, κ_{MW}, we consider the case that our cavity 2 (the comb cavity) is driven by a continuous microwave signal without the existence of the cavity 1. Then, the Hamiltonian of the system follows a single-resonator EO comb model (we set $\hbar=1$ in which $\hbar$ is the Planck constant):

$$H = \sum_{j=-N}^{N} \omega_j a_j^\dagger a_j + \Omega \cos \omega_{MW} t \left(a_j^\dagger a_{j+1} + \text{h.c.}\right)$$

in which a_j ($a_j^\dagger$) is the annihilation (creation) operator of each optical mode j, t is time, ω_j represents the frequency of each frequency mode, Ω is the coupling rate due to microwave modulation and ω_{MW} is the frequency of the microwave signal. We also assume that the frequency modes range from $j=-N$ to $j=N$. Implementing the Heisenberg–Langevin equation gives a set of equations of motion for each mode a_j:

$$\dot{a_j} = \left(-i\omega_j - \tfrac{\kappa_2}{2}\right) a_j - i\Omega\cos\omega_{MW}t \times \left(a_{j+1} + a_{j-1}\right) - \sqrt{\kappa_{e2}}\alpha_{in} e^{-i\omega_L t}\delta_{j,0}$$

in which i is the imaginary unit, κ_{e2}, κ_{i2} and κ_2 ($=\kappa_{e2}+\kappa_{i2}$) are the coupling rate between cavity 2 and the output waveguide, the intrinsic loss rate of cavity 2, and total loss rate of a_j, respectively. The pump power and frequency are denoted by α_{in} and ω_L, respectively. We use the Kronecker delta function $\delta_{j,0}$ to indicate that only the zeroth mode is pumped. Therefore, we write ω_j as $\omega_j=\omega_0+j\times FSR$ in which ω_0 is the resonance frequency of the zeroth mode. By changing rotating frames for each mode $a_j \rightarrow a_j e^{-i\omega_L t} e^{-ij\omega_{MW} t}$, we obtain the simplified equations of motion:

$$\dot{a_j} = \left(i\Delta + i\delta - \frac{\kappa_2}{2}\right) a_j - i\frac{\Omega}{2}\left(a_{j+1} + a_{j-1}\right) - \sqrt{\kappa_{e2}}\alpha_{in}\delta_{j,0}$$

in which $\Delta=\omega_L-\omega_0$ and $\delta=\omega_{MW}-FSR$ are the laser detuning and the microwave detuning, respectively.

The steady state of such a system can be analytically solved. Considering the case that $\Delta=\delta=0$, the equations of motion become

$$0 = -\frac{\kappa_2}{2} a_j - i\frac{\Omega}{2} a_{j+1} - i\frac{\Omega}{2} a_{j-1} - \sqrt{\kappa_{e2}}\alpha_{in}\delta_{j,0}.$$

Note that the equation of motion for the mode with the largest mode number is

$$0 = \left(-\frac{\kappa_2}{2}\right) a_N - i\frac{\Omega}{2} a_{N-1}$$

which gives a relation $a_N = -i\frac{\Omega}{\kappa_2} a_{N-1}$. As a result, the equation for a_{N-1} becomes

$$0 = \left(-\frac{\kappa_2}{2}\right) a_{N-1} - i\frac{\Omega}{2} a_{N-2} - \frac{\Omega}{2}\frac{\Omega}{\kappa_2} a_{N-1}$$

which leads to another relation $a_{N-1} = -i\frac{\Omega}{\kappa_2\left(1+\frac{\Omega^2}{\kappa_2^2}\right)} a_{N-2}$. By iterating the above steps, we obtain the relation for an arbitrary mode a_l with l representing an arbitrary mode number.

$$a_l = -i\frac{\Omega}{\kappa_2}\frac{1}{1+\frac{\frac{\Omega^2}{\kappa_2^2}}{1+\frac{\frac{\Omega^2}{\kappa_2^2}}{1+\frac{\frac{\Omega^2}{\kappa_2^2}}{1+\cdots}}}} a_{l-1}$$

where the total number of the factor $\frac{\Omega^2}{\kappa_2^2}$ is $N-l$. As a result, the equation of motion for the zeroth mode is

$$0 = -\tfrac{\kappa_2}{2} a_0 - i\tfrac{\Omega}{2} \left(-i\frac{\Omega}{\kappa_2}\frac{1}{1+\frac{\frac{\Omega^2}{\kappa_2^2}}{1+\frac{\frac{\Omega^2}{\kappa_2^2}}{1+\frac{\frac{\Omega^2}{\kappa_2^2}}{1+\cdots}}}}\right) a_0 - i\tfrac{\Omega}{2} \left(-i\frac{\Omega}{\kappa_2}\frac{1}{1+\frac{\frac{\Omega^2}{\kappa_2^2}}{1+\frac{\frac{\Omega^2}{\kappa_2^2}}{1+\frac{\frac{\Omega^2}{\kappa_2^2}}{1+\cdots}}}}\right) a_0 - \sqrt{\kappa_{e2}}\alpha_{in}.$$

Simplifying this equation gives

$$0 = \left(-\frac{\kappa_2}{2} - \frac{\kappa_{MW}}{2}\right) a_0 - \sqrt{\kappa_{e2}}\alpha_{in}$$

in which $\kappa_{MW}=\kappa_2\times 2(f_n-1)$ with

$$f_n = 1 + \cfrac{\frac{\Omega^2}{\kappa_2^2}}{1 + \cfrac{\frac{\Omega^2}{\kappa_2^2}}{1 + \cfrac{\frac{\Omega^2}{\kappa_2^2}}{1 + \cfrac{\frac{\Omega^2}{\kappa_2^2}}{1 + \cdots}}}}$$

In the limit of N is a very large number, and we can use the limit of f_n with f defined as $f \triangleq \lim_{n\to\infty} f_n$ and $f = 1 + \frac{\frac{\Omega^2}{\kappa_2^2}}{f}$ to solve the final expression for κ_{MW}, as

$$\kappa_{MW} = \kappa_2 \left(\sqrt{1 + \frac{4\Omega^2}{\kappa_2^2}} - 1 \right).$$

Conversion efficiency analysis using the generalized critical coupling condition. With the expression for κ_{MW}, the single-resonator EO comb system can be simplified to a single mode, which has three loss rates κ_{e2}, κ_{i2} and κ_{MW}. Therefore, the steady-state equations for a coupled-resonator EO comb are

$$0 = -\frac{\kappa_2 + \kappa_{MW}}{2} a_0 - i\mu d$$

$$0 = -\frac{\kappa_1}{2} d - i\mu a_0 - \sqrt{\kappa_{e1}}\alpha_{in}$$

in which d is the pump mode of cavity 1, μ is the evanescent coupling rate between cavities 1 and 2, and κ_{e1}, κ_{i1} and κ_1 ($=\kappa_{e1}+\kappa_{i1}$) are the coupling rate between cavity 1 and input waveguide, the intrinsic loss rate of the cavity 1, and the total loss rate of d, respectively. Note that in the above equation, cavity 1 is pumped instead of cavity 2. Hence, the effective loss rate κ_{1eff} for cavity 1 that is induced by cavity 2 and the output waveguide of cavity 2 is

$$\kappa_{1eff} = \frac{4\mu^2}{\kappa_2 + \kappa_{MW}}$$

and a critical coupling condition occurs when $\kappa_{e1} = \kappa_{i1} + \frac{4\mu^2}{\kappa_2+\kappa_{MW}}$. The output in the through-port waveguide is $d_{out} = \alpha_{in} + \sqrt{\kappa_{e1}}d = \alpha_{in}\left(\frac{\kappa_{1eff}+\kappa_{i1}-\kappa_{e1}}{\kappa_{1eff}+\kappa_{i1}+\kappa_{e1}}\right)$. The amplitude that is lost in the intrinsic loss of cavity 1 is $d_i = \sqrt{\kappa_{i1}}d = \alpha_{in}\frac{2\sqrt{\kappa_{e1}\kappa_{i1}}}{\kappa_{1eff}+\kappa_{i1}+\kappa_{e1}}$. Therefore, the power that flows to cavity 2 can be obtained from

$$P_2 = \left(|\alpha_{in}|^2 - |d_{out}|^2 - |d_i|^2 \right).$$

Finally, the output comb power is dominated by the factor $\xi = \frac{\kappa_{e2}}{\kappa_{e2}+\kappa_{i2}}$, which quantifies the energy going to the output comb channel when light is circulating inside cavity 2. Note that ξ does not include the losses of other frequency modes except for the pump mode back to cavity 1 and the input waveguide, which is negligible due to the off-resonant condition between cavity 1 and cavity 2. For some frequency modes at which cavity 1 and cavity 2 are resonant because of the Vernier effect, the loss is minor since the power of those frequency modes is much lower than the modes close to the pump mode. Thus, the conversion efficiency is

$$\eta = \frac{P_{comb}}{P_{in}} = \frac{P_2}{P_{in}} \times \xi.$$

Therefore the parameter ξ sets the fundamental limit of the conversion efficiency. For example, in this work, cavity 2 is nearly critically coupled to the output comb waveguide, leading to a ~50% theoretical limit of the conversion efficiency. With the expression for P_2, we obtain the final efficiency:

$$\eta = \left(1 - \left(\frac{\kappa_{1eff} + \kappa_{i1} - \kappa_{e1}}{\kappa_{1eff} + \kappa_{i1} + \kappa_{e1}}\right)^2 - \left(\frac{2\sqrt{\kappa_{e1}\kappa_{i1}}}{\kappa_{1eff} + \kappa_{i1} + \kappa_{e1}}\right)^2\right) \times \frac{\kappa_{e2}}{\kappa_{e2} + \kappa_{i2}}.$$

Data availability

The datasets generated and analysed during this study are available from the corresponding authors upon reasonable request.

References

35. Ramelow, S. et al. Strong polarization mode coupling in microresonators. *Opt. Lett.* **39**, 5134–5137 (2014).

Acknowledgements

We thank C. Wang for helpful discussion. This work is supported by AFOSR FA9550-19-1-0376 (A.S.-A.); AFOSR FA9550-19-1-0310 (A.S.-A. and Y.H.); DARPA LUMOS HR0011-20-C-137 (M.Y., L.S., R.C. and M.L.); NASA 80NSSC21C0583 (M.Y. and R.C.); AFRL FA9550-21-1-0056 (N.S.); NSF ECCS-1839197 (D.Z.); ARO W911NF2010248 (Y.H.); DOE DE-SC0020376 (N.S. and M.L.); Harvard Quantum Initiative (HQI) postdoc fellowship (D.Z.); Maxim Integrated (now Analog Devices) (B.B. and J.M.K.); and Inphi (now Marvell) (B.B. and J.M.K.). N.S. acknowledges support by the AQT Intelligent Quantum Networks and Technologies (INQNET) research program. Device fabrication was performed at the Harvard University Center for Nanoscale Systems. The views, opinions and/or findings expressed are those of the author and should not be interpreted as representing the official views or policies of the Department of Defense or the US Government.

Author contributions

Y.H. and B.B. conceived the idea. Y.H. developed the theory and fabricated the devices. M.Y. and Y.H. carried out the measurements. B.B. and Y.H. performed the numerical simulations. Y.H. wrote the manuscript with contributions from all authors. N.S., D.Z., R.C., A.S.-A., L.S. and M.Z. helped with the project. M.L. and J.M.K. supervised the project.

Competing interests

M.Z. and M.L. are involved in developing lithium niobate technologies at HyperLight Corporation. The remaining authors declare no competing interests.

Additional information

Extended data is available for this paper at https://doi.org/10.1038/s41566-022-01059-y.

Correspondence and requests for materials should be addressed to Yaowen Hu or Marko Lončar.

Peer review information *Nature Photonics* thanks Songtao Liu, Xiaoxiao Xue and the other, anonymous, reviewer(s) for their contribution to the peer review of this work.

Reprints and permissions information is available at www.nature.com/reprints.

Extended Data Table 1 | Parameters of the devices

Parameters	Values
Waveguide-cavity 1 coupling κ_{e1}	2π×1.37 GHz
Intrinsic loss rateκ_{i1}	2π×152 MHz
Intrinsic quality factor Q_{i1}	1.2×10^6
Waveguide-cavity 2 coupling κ_{e2}	$2\pi \times 85$ MHz
Intrinsic loss rate κ_{i1}	$2\pi \times 137$ MHz
Intrinsic quality factor Q_{i2}	1.4×10^6
Cavity 1-cavity 2 coupling μ.	$2\pi \times 1.47$ GHz
Mode-coupling rate Ω	$2\pi \times 7.40$ GHz
Modulation index β	0.48π

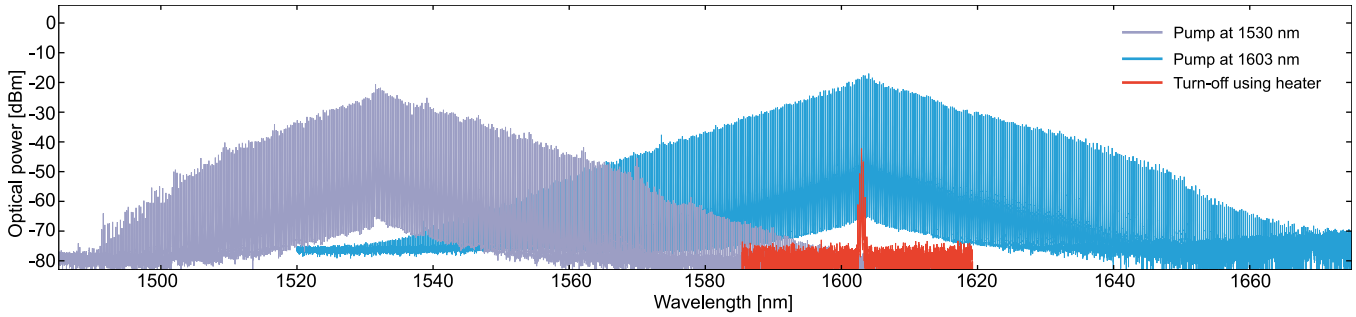

Extended Data Fig. 1 | Tunability of pump frequency and turning on-off using the heater. Spectra of the device pumped at 1530 nm (purple trace) and 1603 nm (blue trace and red trace). By tuning the resonances of cavity 1 to match the resonances of cavity 2, the device can be pumped at different wavelengths. The cut-off at wavelengths that are far blue-detuned (purple trace) is due to TE-TM (transverse electric-transverse magnetic) polarization crossing, which affects the TE-designed cavity 2, and can be minimized by additional dispersion engineering[35]. The comb can also be turned off simply by tuning the resonance of cavity 1 to be mis-aligned from cavity 2. The blue and red traces show the on and off comb states by changing the heater voltages without changing the laser or microwave drive, showing an excellent extinction ratio.

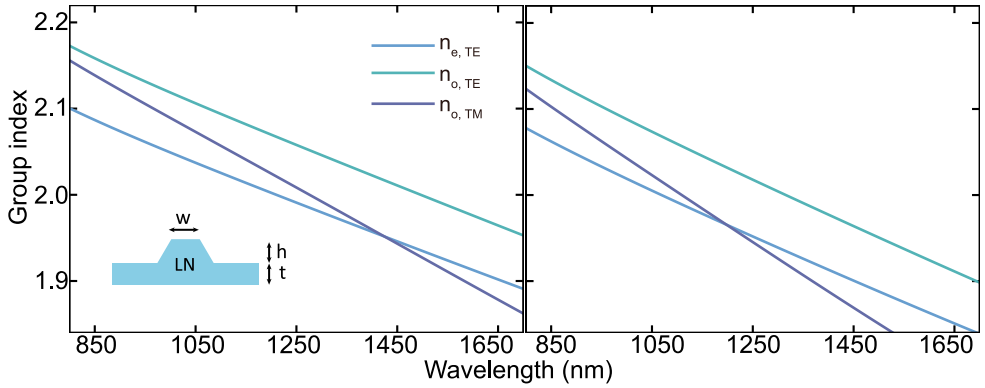

Extended Data Fig. 2 | Minimizing the TE-TM crossing via dispersion engineering. The cut-off of the comb spectrum around 1400 nm originates from the TE-TM polarization crossing. Due to birefringence of lithium niobate, the TE modes that propagate along the y- and z-direction of the thin-film lithium niobate crystal axes have different indices $n_{o,TE}$ and $n_{e,TE}$, respectively, while the indices of TM modes are $n_{o,TM}$ for both directions. When the TE mode circulates inside the micro-resonator, it experiences different averaged TE indices ranging from $n_{e,TE}$ to $n_{o,TE}$ at different bending points of the resonator. As a result, in our current geometry ($w = 1.2\ \mu m$, h = 350 nm, and $\boldsymbol{t} = 250$ nm), the TM mode has an index that is between the value of $n_{o,TE}$ and $n_{e,TE}$ at wavelengths below ~1450 nm (Left panel), leading to a degeneracy between the TM index and averaged TE indices. This index degeneracy can cause polarization-crossing, which can be pushed toward lower wavelength via dispersion engineering. For example, for a geometry with $w = 1.2\ \mu m$, $h = 350$ nm, and $t = 150$ nm, the range that $n_{o,TM}$ is in between the $n_{o,TE}$ and $n_{e,TE}$ is pushed to ~1250 nm.

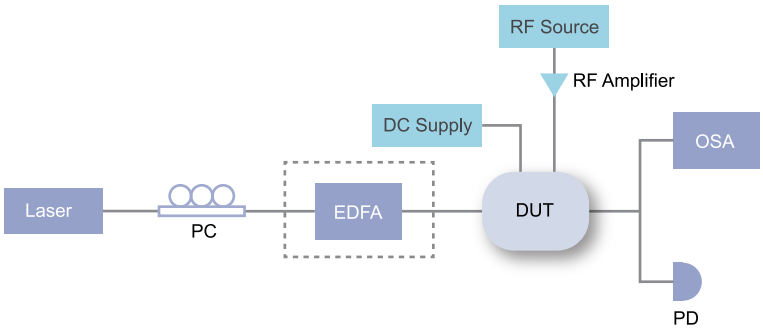

Extended Data Fig. 3 | Measurement setup for Figs. 2 and 3. The coupled-resonator device is characterized using the above setup. In the experiment of Fig. 2b, an EDFA is used to obtain higher pump power. In the experiment of Figs. 2c and 3b, the EDFA is not used. PC, polarization controller; DUT, device under test; EDFA, Erbium-doped fiber amplifier; OSA, optical spectrum analyzer; PD, photodetector.

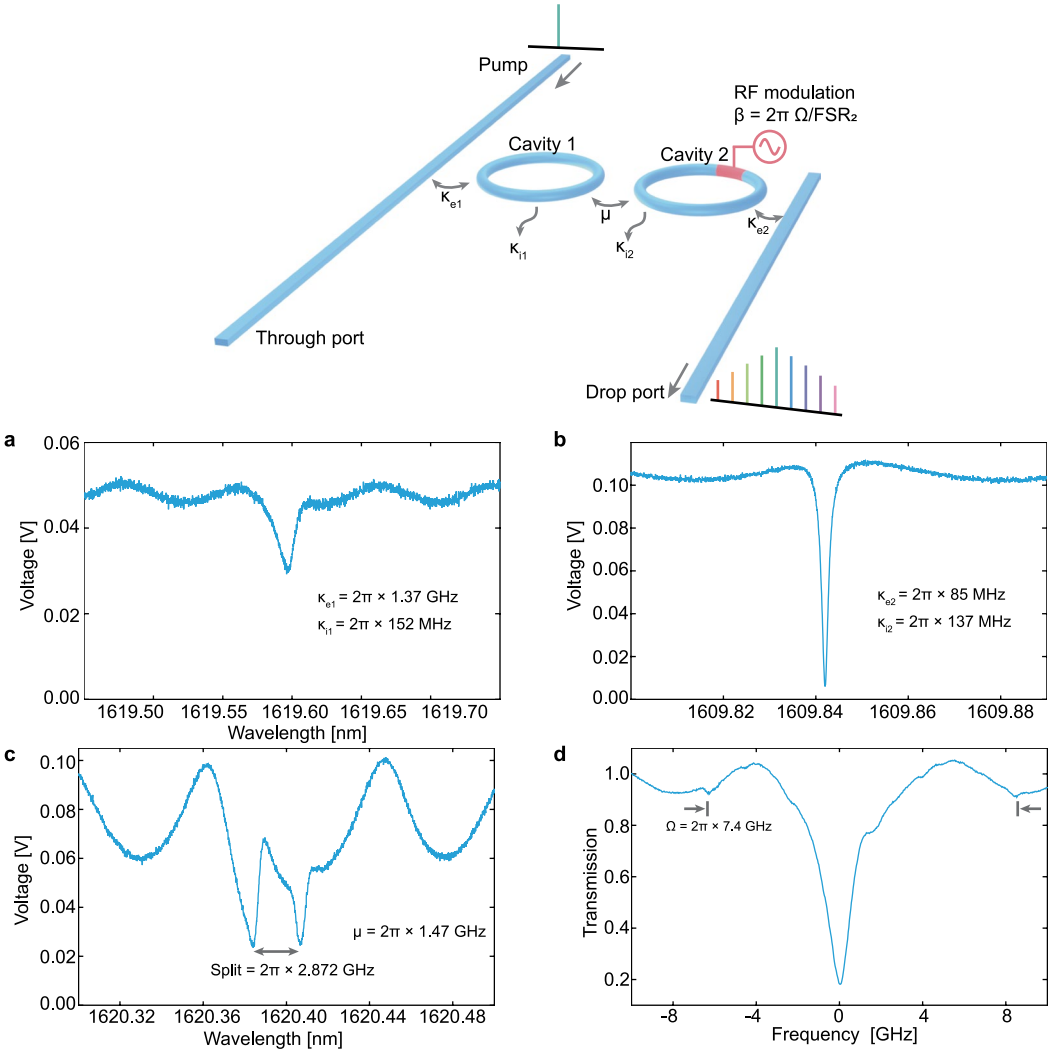

Extended Data Fig. 4 | Device parameter analysis. a, b, Transmission spectrum of a single cavity 1 (a) and 2 (b) with the same fabrication parameters as the coupled-resonator device. **c**, Transmission spectrum of a coupled-resonator device on the through port. **d**, Transmission spectrum of a coupled-resonator device when microwave is on. (c) and (d) are measured on two different coupled-resonator devices with the same fabrication parameters. The background oscillation is due to the Fabry-Perot resonance formed in the bus waveguide due to the reflection at the two facets of the chip. The extracted parameters give a theoretical conversion efficiency of 28%.

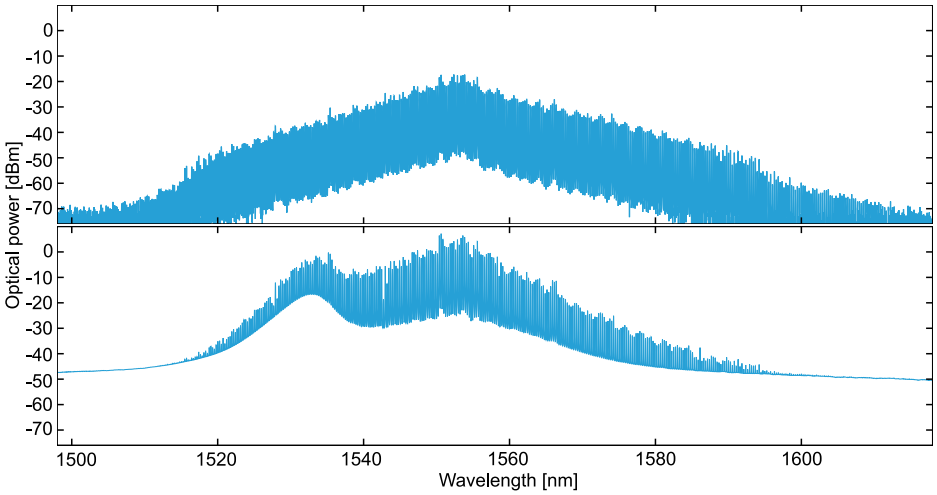

Extended Data Fig. 5 | Frequency spectrum before and after passing the EDFA. The spectrum shows the frequency comb before (top panel) and after (bottom panel) amplification by the EDFA in the time-domain pulse measurement of Fig. 4b.

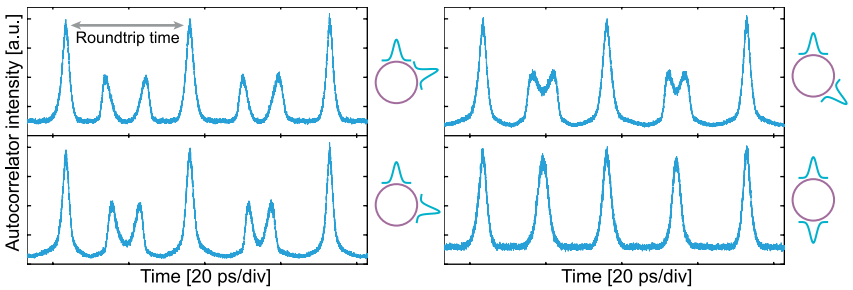

Extended Data Fig. 6 | Tuning the dual-pulse in one roundtrip time. The high conversion-efficiency allows us to measure the signal in the time-domain under varied optical detuning. Unlike dark-pulse Kerr combs or platicons in a coupled-resonator Kerr frequency comb generator[20], which exhibits a completely different mechanism in both spectral and temporal domains compared to their single-resonator counterparts, our coupled-resonator structure preserves the time-domain features of the single-resonator EO combs. The output signal shows that there are two pulses in one round-trip time and the delay between the two pulses can be tuned by changing the optical detuning, which is identical to the conventional single-resonator EO comb.